GEOLOGY

First field evidence of the electrical multipolar nature of volcanic aggregates

Stefano Pollastri, Eduardo Rossi*, Costanza Bonadonna

The description of the formation of ash aggregates is crucial to our understanding of tephra dispersal and, therefore, to the forecasting of volcanic ash concentration in the atmosphere. Regardless of the importance of electrostatic processes, particle and aggregate charge is of complex determination both in the field and in the laboratory. We have measured the bulk charge carried by single aggregates at Sakurajima volcano (Japan) by inverting the sedimentation trajectory across two high-voltage copper plates filmed using a high-speed camera. Some aggregates were filmed during their breakage caused by the external electric field, which revealed the presence of inner highly charged multipoles with bulk charge up to one order of magnitude larger than the bulk aggregate. This electrical multipolar nature reveals the key role played by multipoles in aggregate formation and the shielding effect of aggregation on particle charge.

INTRODUCTION

Explosive volcanic eruptions release into the atmosphere a large amount of fine ash (tephra with diameter <63 μm), affecting public health and infrastructure functional to a wide range of economic sectors (*1*). Because a relevant amount of fine ash sediments are aggregates (*2*), a full understanding of aggregation mechanisms is necessary to forecast ash concentration in the atmosphere and mitigate the associated risk (*3*–*5*). In the past three decades, an increasing amount of laboratory and field observations have suggested that electrostatic forces may play a leading role in the aggregation of volcanic ash (*2*, *6*–*9*). As a consequence, many efforts have been dedicated to laboratory and numerical investigations of ash electrification (*7*, *10*–*13*). The presence of a bulk charge Q on the surface of volcanic ash is believed to influence both the binding mechanisms (*8*) and the collision rate between particles (*14*, *15*). At the macroscopic scale, a well-known consequence of the highly charged nature of ash particles can be found in the ubiquitous observation of volcanic lightning inside volcanic plumes (*16*–*19*). At the microscopic scale, charge rearrangement among atoms or the production of free electrons involves several distinct processes (*20*, *21*), such as tribocharging due to particle collisions (*22*), fractoemission after multiple breakages (*23*), and release or absorption of ions contained in the surrounding gas and the induced charge due to background potentials (*24*). In addition, Woods *et al.* (*25*) have recently shown that volcanic ash is a good insulating material within the range of explored values of relative humidity (RH) (i.e., RH < 31.6%). This suggests that volcanic ash can easily hold the charge and that several electrified patches of different signs can be present on the surface of ash particles. This is likely to hold also for larger values of RH than the ones investigated by their experimental apparatus, although further investigations are required.

Volcanic eruptions represent a challenging environment to be fully reproduced with laboratory experiments due to (i) the presence of multiple charging processes occurring at the same time; (ii) time scales for charge generation that span values from milliseconds to thousands of seconds; (iii) highly energetic particle-particle collisions; (iv) highly energetic fragmentation processes; and (v) a wide range of particle size and composition. Therefore, field experiments still represent a unique opportunity to study ash electrification in a real natural event and to provide a reliable benchmark to better constrain both laboratory experiments and numerical investigations. However, the direct measure of Q in a natural context is a challenging task due to a variety of aspects, including the complexity of the used techniques (e.g., need of a movable high-voltage apparatus), the environmental conditions (e.g., potentially windy and wet), and the accessibility of favorable/optimal sampling sites (e.g., right under the dispersal axis of the volcanic cloud). It is thus expected that, so far, only three field studies on this topic have been described in literature and that none of them measured the bulk charge associated with single falling objects (i.e., particles or aggregates) but only average values of the charge-to-mass ratio ($\frac{Q}{m}$) relative to bulk quantities. During the 1941 eruption of Mount Asama (Japan), Hatakeyama found average values of $\frac{Q}{m} \approx -4 \times 10^{-7}$ C kg^{-1} by using a Faraday cup setup (*26*). At Sakurajima volcano (Japan), Gilbert *et al.* (*27*) directly measured values of Q associated with bulk quantities of ash by means of two different setups, e.g., a high-voltage copper plate (HVCP) apparatus coupled with an electrometer and a Faraday cup combined with an electrometer; they found that the absolute charge-to-mass ratio was between -5×10^{-4} and $+6 \times 10^{-4}$ C kg^{-1}. Last, Miura *et al.* (*28*) used an HVCP during tephra fallout at Sakurajima volcano to produce a deflection in the trajectory of charged ash that allowed them to determine $\frac{Q}{m}$ from the horizontal displacement; they found that the absolute $\frac{Q}{m}$ was between -4×10^{-5} and $+4 \times 10^{-5}$ C kg^{-1}. Despite their historical importance, these studies still leave some fundamental open questions that need to be addressed: (i) How much charge can be carried by single particles and single ash aggregates? (ii) How does the electric charge contribute to the formation of ash aggregates? (iii) Is it possible for ash aggregation to influence macroscopic electric phenomena such as volcanic lightning?

Here, we present a new setup that uses the deflection technique (*29*–*31*) to measure the bulk charge Q carried by individual ash aggregates settling during tephra fallout, obtained by means of the simultaneous combination of HVCP and a high-speed camera (HSC) videography (Fig. 1). The HSC allows for a complete reconstruction

Department of Earth Sciences, University of Geneva, Rue des Maraichers 13, Geneva, Switzerland.
*Corresponding author. Email: eduardo.rossi@unige.ch

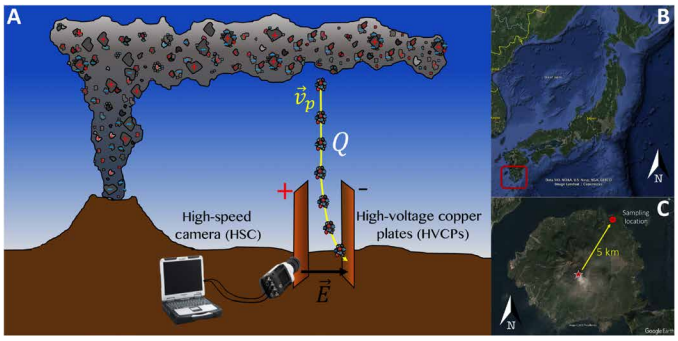

Fig. 1. Field setup and volcanic context. (**A**) Sketch of the deflection technique used to measure the net electric charge (*Q*) carried by single ash aggregates. Naturally electrified ash aggregates are recorded with an HSC during their sedimentation across two HVCPs. The unknown *Q* on the single aggregate can be then derived by inverting the trajectory, once the terminal velocity, aggregate size, and density have been measured. (**B**) Regional location of Sakurajima volcano (Japan). (**C**) Sampling location and distance from the vent of measurements (longitude: 130.6894444; latitude: 31.6192222).

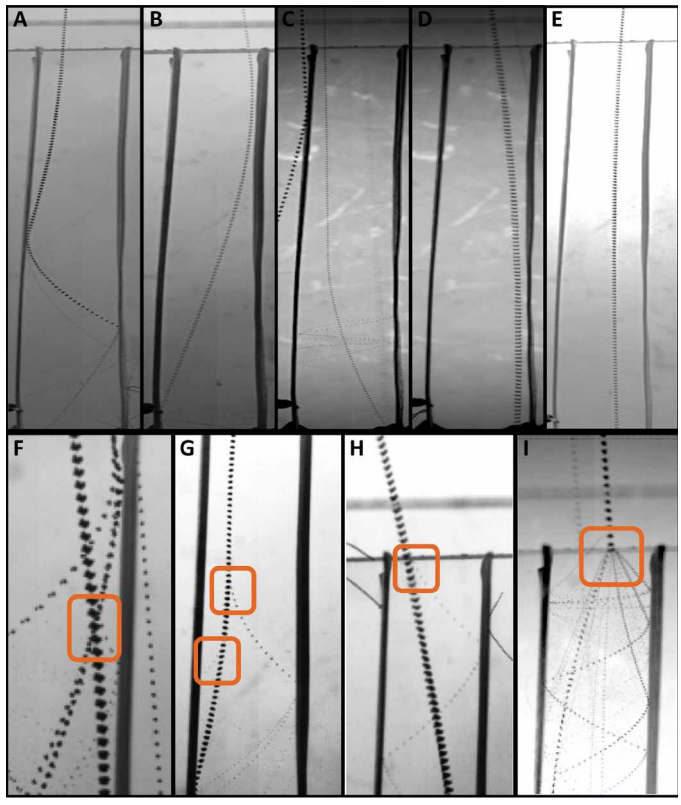

Fig. 2. Charged aggregates and multipoles. Raw images of aggregates falling within the HVCP recorded with the HSC (composition of multiple frames). (**A** to **E**) Aggregates not fragmented by the external electric field. (**F** to **I**) Aggregates fragmented by the external electric field: AF1 (F), AF2 (G), AF3 (H), and AF4 (I). The orange box indicates the moment of breakage of the original aggregates in one or more fragments.

of the dynamics of the motion inside the copper plates. Aggregates are also known to disaggregate (*32*) upon deposition, but their disaggregation was never correlated to a controlled electric field. As a result, this represents a unique study, which is part of a larger field campaign for the general characterization of ash aggregates (*33*). The measurements were carried out at Sakurajima volcano (Japan) for about 50 min starting at 2:24 p.m. (Japanese local time) of 26 November 2019, about 17 min after the beginning of a small-moderate Vulcanian explosion occurred at Minamidake crater. The sampling location was placed 5 km downwind from source (Fig. 1), and the maximum plume height associated with the eruption was about 2600 m above the vent (3450 m above sea level). This technique measures the mass and the charge of single falling ash aggregates by inverting the recorded trajectory both before their entrance in the HVCP and within the HVCP (Fig. 2). It also allows for a comprehensive characterization of the size and terminal velocity as well as of the structure of each single aggregate for which the charge has been measured. The use of this technique revealed unexpected aspects of the complex nature of electrification within ash aggregates. The disaggregation of settling aggregates induced by the applied external electric field (*32*) provides a first clue that ash aggregates may be formed by macroscopic electric multipoles (Fig. 2, F to I), as already has been found in other scientific fields, e.g., planetary formation and pharmaceuticals (*34*, *35*). Such a discovery helps to understand the formation and growth of ash aggregates given that electrical multipoles were found to affect the stability of their structure and formation. In addition, the multipolar structure of ash aggregates can have visible implications at the macroscopic scale on the formation of volcanic lightning, as discussed in the following sections.

RESULTS

Computation of the bulk charge carried by ash aggregates as a function of the aggregate type

The deflection technique, designed to quantify the bulk electric charge carried by a given object (*29*–*31*), is applied here specifically to volcanic ash aggregates, which are the main goal of this study (Fig. 2). In addition, combined with HSC videos, it also allows for the simultaneous measurement of fundamental kinematic and dynamic properties of particles, such as their terminal fall velocity and size. All this information can be combined to provide a better understanding of the relationship between ash electrification and ash aggregation. We identified the typology of 44 aggregates collected on 26 November 2019 that did not break as a result of the applied HVCP electrical field (ash clusters, PC1; particle clusters, PC2; cored clusters, PC3) based on the classification of Brown *et al.* and Bagheri *et al.* (*2*, *36*), as well as on the description of associated typical terminal velocity and density of Diaz Vecino *et al.* (see sections S1 and S2) and Gabellini *et al.* (*33*, *37*) (compare figure 5A of their work). PC1 aggregates consist of fine ash particles (<63 μm) of similar size, PC2 aggregates consist of a coarse ash particle (typically between 63 and 2000 μm) covered by scattered fine ash, and PC3 aggregates consist of a coarse ash particle covered by a thick shell of fine ash (*2*, *33*, *37*).

The bulk charge (*Q*), the surface charge density (σ_b), and net charge-to-mass ratio of these 44 aggregates in addition to 7 aggregate fragments are shown in Fig. 3 as a function of the aggregate type (error bars on the values are displayed in section S3). It is worth noting that the surface charge density (σ_b) is calculated assuming that the net charge is distributed on the surface of a sphere with the same diameter of the aggregate. This is to be considered as a minimum

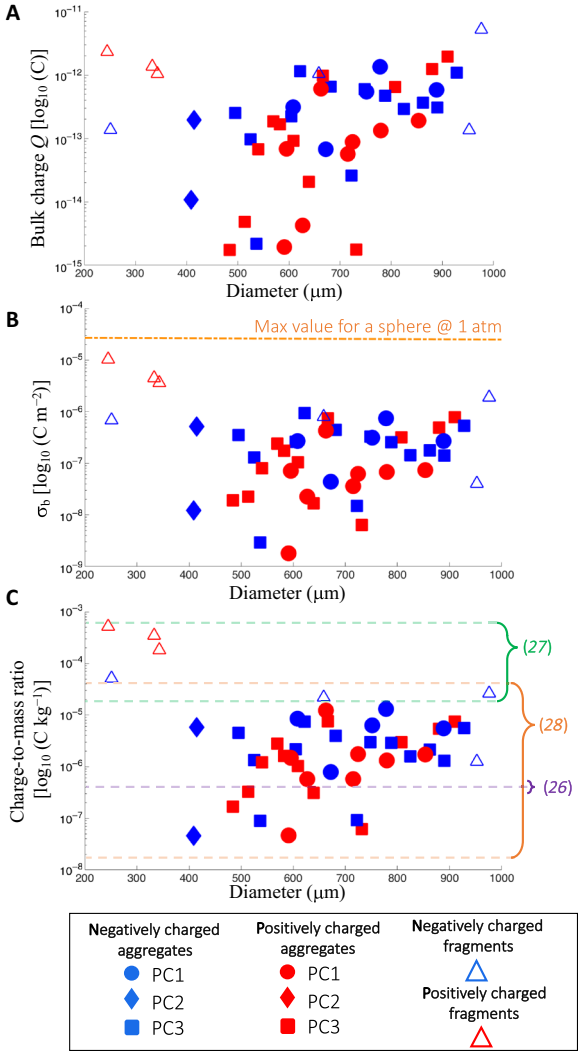

Fig. 3. Bulk charges, surface charge density, and charge-to-mass ratios. Electrical properties for fragmented and not fragmented aggregates as a function of the aggregate type: (**A**) the bulk electric charge (*Q*); (**B**) the charge surface density (σ_b) (normalized assuming the surface of a sphere with equivalent diameter of the aggregate); and (**C**) the charge-to-mass ratio, with the indication of ranges of values reported in literature (*26*–*28*).

value because the actual surface of aggregates is porous and irregular. As a result, the values reported in Fig. 3B should be regarded as the low bound for the surface charge density. The bulk charge carried by the observed aggregates comprises between 10^{-15} and 2×10^{-12} C, the surface charge density spans values between 2×10^{-9} and 10^{-6} C m^{-2}, and the charge-to-mass ratio comprises between 4×10^{-8} and 2×10^{-5} C kg^{-1}.

Aggregates with diameters larger than 730 μm are associated with a bulk charge larger than 10^{-13} C, surface charge density larger than 5×10^{-8} C m^{-2}, and charge-to-mass ratio larger than 10^{-6} C kg^{-1}. However, no clear correlation exists between aggregate type, bulk charge, and polarity. According to the size-dependent bipolar charging (SDBC) process, triboelectric charging produces, on average, small particles negatively charged and large particles positively charged (*38*–*40*). This has also been confirmed for ash particles, where particles with diameter <100 μm show higher probability of being negatively charged by triboelectric charging (*11*, *41*). However, PC1 (dominated by fine ash) and PC3 (characterized by a coarse-ash core) span the same range of bulk charges, and no visible trend can be seen with respect to the aggregate size. Unfortunately, the reduced number of PC2 aggregates observed at our location does not allow for significant conclusions to be drawn about this aggregate type. The lack of a clear footprint for the electrical charge associated with aggregate type may indicate that the charge carried by the inner components is somehow randomly distributed among all the objects and it is not a size-dependent process. This may occur because tribocharging is combined with other non–size-dependent processes of charge generation, such as the fractoemission (*41*).

Observation and quantification of the electrical multipolar nature of ash aggregates

The presence of a strong electric field within the HVCP (e.g., 495 ± 73 kV m^{-1}) may lead not only to a deviation of the trajectory for falling aggregates but also to the breakage of the original aggregates. When this happens, important insights into the electrical properties of the internal structure can be obtained, such as the presence of highly charged subregions of well-defined polarity, hereafter named electrical multipoles. The breaking of the original aggregate structure is a quite rare event in our observations: It has been recorded only for three aggregates in the dataset, which represent 6% of the analyzed aggregates (i.e., 3 of 47 aggregates have resulted in 7 fragments). Hereafter, the aggregate fragments are named as AF1, AF2, and AF3 and displayed in Fig. 2 (F to H). AF2 showed a double breakage due to the external electric field along the trajectory (Fig. 2G). In addition, a fourth aggregate revealed the presence of electrical multipoles (Fig. 2I), for which, unfortunately, the computation of the charge was not possible because of the impact with the protective glass of the HVCP. Terminal velocity and size of these broken aggregates are as follows: $v_t = 1.97$ m s^{-1} and $d_A = 792$ μm for AF1; $v_t = 1.97$ m s^{-1} and $d_A = 792$ μm for AF2; and $v_t = 1.75$ m s^{-1} and $d_A = 1097$ μm for AF3. PC1 are assumed to be characterized by a spatially isotropic density within their structure. On this basis, we associate the same density of the original aggregate to each broken fragment. The charge is then evaluated with the same procedure implemented for not broken aggregates (see Materials and Methods) (Table 1). The seven observed aggregate fragments show high values of charge, charge surface density, and charge-to-mass ratios typically higher than whole aggregates (Fig. 3C).

DISCUSSION

The results of our analyses provide relevant insights into the formation and stability of PCs, i.e., volcanic aggregates for which binding is not dominated by liquid water. First, we have shown how PCs consist of a combination of multipoles with a higher electric field with respect to the bulk aggregate; such a structure enhances the stability of the aggregate. Second, the electric field of individual multipoles is reduced by the shielding effect of the aggregate with possible consequences on lightning generation. These aspects are detailed below.

From single-particle electrification to the electrical multipolar nature of ash aggregates

The HSC videos of aggregates falling within the HVCP have revealed that the bulk electric charge carried by not-broken aggregates

spans more than three orders of magnitude, from almost neutral values (~10^{-15} C) up to significant charge (~10^{-12} C). A large variability of the dataset is also confirmed by the charge-to-mass ratio (~10^{-8} to 10^{-5} C kg^{-1}), a more significant parameter that combines the response to the external electric field and the inertia of the aggregate. In addition, considering that the RH in the atmosphere on 26 November was quite high [i.e., between 60 and 99%; see figure 6K in (*33*)], we cannot a priori exclude that the presence of conductive water bridges over the surface of ash particles may have acted as a discharging mechanism in specific moments of aggregates formation: This implies that the values for charge should be seen as lower bounds with respect to a dry situation (i.e., RH <31%), for which Woods *et al.* (*25*) already demonstrated that volcanic ash is a very good insulator. However, Fig. 3C also shows a good overlapping of our results and the ones previously obtained by Gilbert *et al.* (*27*) in different days and weather conditions for RH (e.g., 33 to 91%), which indicates that discharging due the presence of liquid bonds, if present, does not significantly affect the final results.

Although ash aggregates show a wide range of electrical properties, and neutral or poorly charged aggregates are common, their inner parts (i.e., the multipoles) seem to be characterized by a much larger electric charge, as demonstrated in Fig. 3 and previously found by other authors for the similar eruptions at the Sakurajima volcano (*27*). Moreover, the sharp step around 400 μm that separates in Fig. 3C AFs and PCs indicates that the observed differences cannot be interpreted as a smooth consequence of the geometrical scaling of the mass and the charge as functions of the diameter.

This is a key result of our analysis regardless of the potential coexistence of other nonelectrostatic binding mechanisms. The inversion algorithm on the fragments and the consequent evaluation of the charge considers the initial condition over position and velocity of the fragments once the breakage has already occurred. The presence of additional sticking mechanisms within the parent structure only influences the stability of the aggregate before the breakage and the chance of breakage but not the final values of the charge and their polarity in the ash fragments.

Comparing our results with the existing literature, it is interesting to notice how the upper bound values of charge-to-mass ratios measured by Gilbert *et al.* (*27*) (e.g., $\pm 5 \times 10^{-4}$ C kg^{-1}) should probably be interpreted, according to Fig. 3C, as the result of the impact of highly charged inner aggregate fragments to the surface of the copper plates, more than to the global net charge of the aggregates. On the other hand, the results obtained by Hatakeyama with a Faraday cup apparatus (*26*) and by Miura *et al.* (*28*) with a deflection technique not based on the use of HSC are compatible with bulk charges carried by whole aggregates (Fig. 3C).

A better understanding of the charge carried by aggregates and single fragments represents a step forward also for the theoretical description of ash aggregation and, ultimately, the forecasting of ash concentration in the atmosphere. So far, theoretical models usually treat ash aggregation in terms of collision and sticking kernels: The former describes the collision rate among particles according to well-defined assumptions on the dynamics of the collisions (*15*); the latter describes the probability of a successful impact that leads two particles to stick, a condition that occurs if the relative kinetic energy of the impact is dissipated. Last, the evolution in time and space of a population of particles is obtained combining the information of the kernels within an advection-diffusion-reaction (ADR) scheme. The electrostatic forces that result from charges carried by single particles and aggregates both affect the collision and the sticking kernel. For instance, Pollastri *et al.* (*14*) recently showed that the presence of a net charge increases the amount of fine particles that can be collected by the aggregate, if compared to neutral case. In particular, Coulomb interactions can significantly increase the volumetric flow rate (i.e., the collision kernel) of opposite charged fine particles; on the other hand, they decrease the sticking efficiency among larger objects [see sticking maps in (*14*)]. It is thus evident how the initial conditions on the charge attributed to single ash particles in ADR models require a particular attention and can significantly affect the final outcome of the forecast. Our observations indicate that the charge over mass associated with AF1, AF2, and AF3, which coincide with the upper limits found by Gilbert *et al.* (*27*), should probably be considered as more representative of the early stages of aggregation. Using lower values, such as the charge-per-unit mass carried by aggregates, could lead to underestimating the effects of the electrostatic forces on the collisional and sticking kernels.

Our results, combined with previous findings (*26*–*28*), shed light on the hidden nature of the electrical composition of ash aggregates. A possible scenario that can explain our observations is summarized as follows (Fig. 4A): (i) Initially, particles are highly charged mostly because of fractoemission processes in the magma-fragmentation phase and/or to the triboelectrification associated with collisions that occur in the volcanic conduit and/or jet (*8*); (ii) the early stage of aggregation is dominated by collisional processes mostly due to turbulence that creates small clusters of randomly charged particles (hereafter named the seeds) that form stable structures with a defined net polarity; (iii) as the volcanic plume rises toward the neutral buoyancy level (NBL) and starts the radial spreading of the cloud, additional collisional mechanisms characterize now the formation of larger agglomerates. Depending on the size of the seed and the coupling with the flow, collisions here can be dominated either by sedimentation or by turbulence. At this stage of aggregation, multiple seeds are combined together in a unique aggregate, which is the result of several multipoles with a global electric field that is generally reduced with respect to both the single seeds and the initial single particles. Nevertheless, this scenario does not exclude that, even for PCs, additional binding mechanisms can play a role in their formation and stability. For instance, it is widely accepted that liquid bonds at the microscopic scale, i.e., in the absence of a macroscopic water layer, can act as a dissipation mechanism for particle-particle collisions, or that the presence of salt

Table 1. Charge carried by single ash fragments. Charge conservation measured for aggregate fragments AF1, AF2, and AF3. CI, confidence interval; n.a., not applicable.

Sample	Aggregate (pC) [95% CI]	Fragments (pC)	
		Positively charged [95% CI]	Negatively charged [95% CI]
AF1	−1.36 [−3.30, −0.67]	2.31[1.41, 8.10]	−5.24[−12.64, −2.88]
AF2	0.61 [0.29, 1.5]	1.04[0.50, 4.09]	−1.05[−2.77, −0.53]
			−0.14[−0.24, −0.10]
AF3	n.a.	1.36[0.62, 4.94]	−0.13 [−0.30, 0.08]

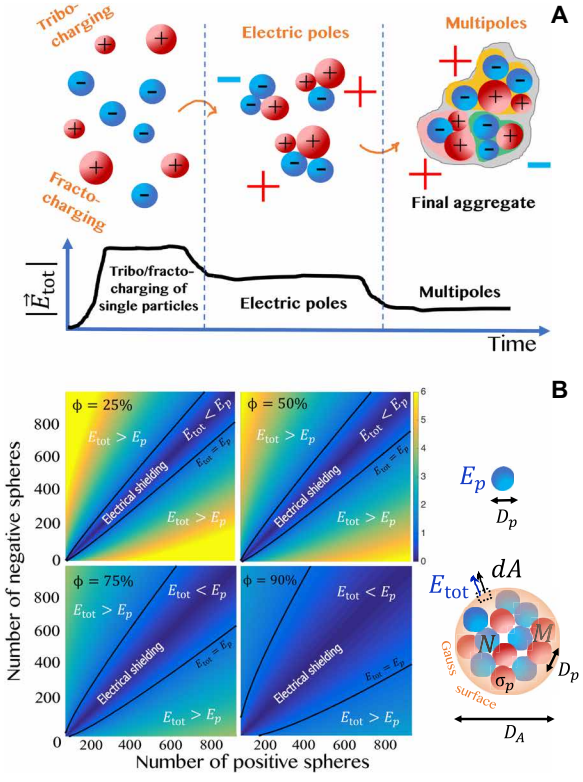

Fig. 4. Formation of electrical multipoles and electrical shielding due to ash aggregation. (**A**) Scenario behind the formation of the observed aggregates. An initial population of single particles is highly charged because of tribo and fracto charging phenomena that may occur in the fragmentation phase and in the collisional processes within the volcanic conduit and jet. Small clusters of aggregates with well-defined polarities (monopoles) are formed in the initial phase of aggregation (seed). The final stage of aggregation leads to an aggregate that is composed of several multipoles that result in a globally neutral or poorly charged object. (**B**) Electrical shielding due to aggregation of nonconductive ash particles for PC1 made of spheres with equal diameter D_p, surface charge density σ_p, and electric field E_p. The global electric field E_{tot} is shown as a function of the aggregate porosity ϕ and the number of positive and negative spheres within the aggregate. Electrical shielding is defined as an overall decrease of the electric field initially carried by single particles (E_p) due to aggregation phenomena (i.e., $E_{tot} < E_p$).

bridges and their consequent evaporation can result in solid bonds among inner particles of the aggregates (*32*).

In this framework, PCs are mostly seen as a combination of electrical multipoles that enhance the stability of the structure. For what concerns the stability of the aggregate, a key role is also played by the polarization forces that naturally arise when a medium with high electric constant is taken into account. Lee *et al.* (*34*) showed that, if the spatial configuration of the components generates favorable arrangements of the polarization, the polarization forces can stabilize even structures formed mostly by particles of the same charge and sign (see their figure 4C).

The electrical shielding due to ash aggregation: Consequences at the macroscale

The field observations discussed in the previous section reveal how the charge-per-unit mass carried by ash aggregates is generally much smaller than the one associated with their inner components, with values comprised between one and four orders of magnitude less (Fig. 3C). This evidence, which was possible thanks to the use of the HSC, introduces the idea that aggregation processes tend to create structures that, in the end, are more electrically neutral than the initial population of single particles. This suggests also that the largest values of charge-per-unit mass already reported in the previous literature (*27*, *28*) should probably be identified as carried by ash fragments more than bulk aggregates which, on the contrary, are probably more poorly charged than previously thought. Similar results have been observed, for example, in the formation of the protoplanetary disks, where the formation of aggregates dominated by tribocharging the SDBC and the polarization in the dielectric lead to stable configurations of overall neutral aggregates (*34*).

Starting from this scenario, we wonder about the consequences of ash aggregation on the final electric field of the whole aggregate, and, lastly, how this influences at the macroscopic scale the electrical phenomena that frequently characterizes the entire volcanic plume, such as volcanic lightning. In particular, given that PCs can be described in terms of clusters of multipoles, we investigate whether and how aggregation can reduce or enhance the total electric field of the aggregate ($\vec{E}_{tot}$) and how the porosity affects the final results.

A rigorous description of the electric field produced by a set of dielectric charged particles should take into account the effects of the polarization of the volcanic ash (*42*, *43*). However, here, a simplified example is proposed for the sake of discussion, following as an analogy that has been proposed for the electrification of exoplanetary clouds (*43*). In our example, a PC1 aggregate of diameter d_A is made of $M + N$ spheres of equal diameter d_p, M with positive surface charge density $\sigma_p = \varepsilon E_p$, and N with negative surface charge density $-\sigma_p$, where E_p is the electric field at the surface of a single particle (see Fig. 4B). The first Maxwell's equation for electromagnetism (i.e., the Gauss law) can be written as follows

$$\int_S \vec{E}_{tot} \cdot d\vec{A} = \frac{\sum_j^M |\sigma_p| S_j^+ - \sum_i^N |\sigma_p| S_i^-}{\varepsilon} \quad (1)$$

where $S_i^- = \pi d_p^2$, $S_i^+ = \pi d_p^2$, $\varepsilon = \varepsilon_r \cdot \varepsilon_0$, ε_r is the relative dielectric constant of the gas, and ε_0 is the permittivity of the vacuum. We consider a spherical Gaussian surface with radius $r = d_A/2$, and, for the sake of simplicity, we assume that $\vec{E}_{tot}$ is radially oriented and only dependent on r. After some algebra, the electric field at the surface of the aggregate can be thus related to the electric field carried by a single component (E_p)

$$\frac{E_{tot}}{E_p} = \frac{(M - N)}{\left(\frac{d_A}{d_p}\right)^2} \quad (2)$$

We assume now that the particle packing inside the aggregate follows the relation proposed by Lane *et al.* (*44*) for laboratory experiments involving PC1 objects (see their equation 5)

$$\frac{d_A}{d_p} = \left(\frac{N_{tot}}{1 - \phi}\right)^{1/3} \quad (3)$$

where $N_{tot} = M + N$ and ϕ is the aggregate porosity. Combining Eqs. 2 and 3, the ratio $\frac{E_{tot}}{E_p}$ can be lastly expressed in a closed analytical form

$$\frac{E_{tot}}{E_p} = \frac{(M-N)}{\left(\frac{M+N}{1-\phi}\right)^{2/3}} \quad (4)$$

Equation 4 is plotted for four values of the porosity (e.g., ϕ = 25, 50, 75, and 90%) and a number of particles between 1 and 1000 (Fig. 4B). As expected, in general, the overall electric field E_{tot} can be larger or smaller than the one carried by the single particles, at least under the assumptions considered in our analysis. However, Fig. 4B suggests that aggregation is more likely to reduce the bulk electric field as the porosity increases: We call this effect the electrical shielding (i.e., $E_{tot} < E_p$).

Following a Lagrangian perspective, the porosity of the PCs increases as the collisional processes evolve in time. For example, Rossi and Bonadonna (*45*) have recently quantified that PC1 type aggregates can have a porosity that evolves in time from negligible values (e.g., <10%) up to a maximum 40% plateau for a tight packing and a 70% plateau for a loose packing. We thus expect that the electrical shielding is actually promoted in those regions of the volcanic plume far from the vent and the jet region, where the aggregate can be made by sufficiently high values of porosity (e.g., at the NBL and in the umbrella spreading).

As recently reviewed by Cimarelli and Genareau (*21*), the study of volcanic ash electrification has its early origin from the impressive records of volcanic lightning during historical eruptions, as for example, reported by Pliny the Younger for the AD 79 eruption at Mt. Vesuvius. The high electrical activity in the eruptive events implies a strong link between the physics of charge generation at the microscale and the final phenomena observed by the naked eye at the macroscopic scale, i.e., the lightning (*18*, *19*, *46*). Following the logical path from micro to macro, the electrical shielding due to ash aggregation may thus have visible consequences also at the macroscopic scale of the volcanic plume and cloud. The increased neutralization of the bulk charge of the single aggregate due to ash aggregation, as observed in the present work, can finally reduce the overall probability of the dielectric breakdown in the gas mixture, resulting in a lower probability of lightning generation. This is supported by the lack of evidence of a strong link between the amount of lightning and ash concentration in plume and cloud (*46*).

MATERIALS AND METHODS

Field apparatus

The setup used for the quantification of the electric charges on the falling aggregates at Sakurajima volcano (Japan) is made of two main parts: (i) an electrostatic generator that charges two rectangular copper plates at a high voltage difference; (ii) an HSC to record aggregate trajectories between the copper plates (see section S4). The charge carried by each aggregate is then derived from the inversion of the recorded path from the equation of motion. In addition, a portable meteorological station was installed at the same location of the experiments (Fig. 1).

The choice of not using a dc power supply is related to the need of having a compact, flexible, and transportable apparatus that can reach high voltages and at the same time guarantee a high level of safety even in the complex environment of volcanic fallout. The electrostatic generator used in our investigations is a modern version of the Wimshurst electrostatic machine (WEM). The model used here has been built by the Sparkit company (http://sparkitelectrostatics.com/). To adapt the WEM to the complexity of a field campaign associated with a volcanic eruption, we largely modified the hardware and the software of the original Sparkit design as shown in section S4. In our version, the WEM is controlled by an Arduino Mega 2560 v3 that runs the two dc motors of the machine according to the software loaded on the ATmega2560 chip of the board. Several programs can be activated by means of an external joystick, such as a testing routine, a routine where the WEM runs for a fixed amount of time (set by the user), and a continuous running program. In the field activities, we mostly used the continuous running program to get a stable electric field within the copper plates. The WEM electrodes are attached to two copper plates of length L = 13.3 cm and width W = 4.0 cm with a gap of d = 1.8 cm between them, which is basically equivalent to a capacitor (also named condenser) with air as dielectric. The design of the condenser satisfies three basic requirements: First, the electric field inside the HVCP, $\vec{E}_{int}$ (here assumed along the horizontal axis in the field of view (FOV) of the camera, i.e., $\vec{E}_{int} = E_{int}\hat{x}$), must cover a sufficiently wide region of space to have enough time to deviate aggregates from their original trajectory; second, sparks due to electrical breakdown must be avoided; last, there must be enough space between the plates to have good changes for particles to fall inside the condenser, even with a low- to moderate-intensity tephra fallout. The loss of charges due to continuous Corona discharging with air is not a problem as long as the apparatus is capable of replacing them and producing a constant and reproducible electric field inside the capacitor. To minimize the uncertainty on the final results, a great attention has been posed in constraining the actual electric field between the plates during the observations. We adopted the strategy to directly measure the electric field before, during, and after the ash fallout by means of three separate measurements obtained using two completely independent techniques (see next sections). This approach guarantees a high degree of reliability on the value of $\vec{E}_{int}$.

In sizing the plates, we assumed an expected charge of the same order of magnitude to what is observed in (*27*). To test the charging process of the WEM during the experiments, a metal sphere was regularly introduced between the plates. The video analysis of the resulting oscillatory motion of the sphere confirmed the good stability of the electric field generated by the instrument (see below). The copper plate located on the left in the FOV of the camera was positively charged, and the right one was negatively charged: This resulted in a deflection toward $-\hat{x}$ for negatively charged aggregates and toward $+\hat{x}$ for positively charged ones. The HSC that was placed in front of the capacitor plane is a Phantom M110 camera with a 60-mm Macro f2.8 controlled by a Panasonic Toughbook laptop. The distance between the camera and the capacitor assures that both the copper plates and a 2-cm margin of empty space above them were displayed on the sensor of the camera. Having a free falling space before entering in the electric field is a key aspect in the technique because some dynamical properties of the falling aggregates are derived from the evaluation of the terminal velocity, such as the mass and the bulk density. To ensure optimal light conditions in the recording, a high-intensity 6 × 4 light-emitting diode array and a holographic diffuser with transmission efficiency of >85% were placed behind the capacitor to backlight the camera field. The sample rate of the HSC has been set to 1500 frames per second (fps) that

for ash falling at an expected maximum velocity of ≈3 m/s ensures around 70 frames for the fastest-falling objects. This number of frames gives an unbiased description of the trajectory in the FOV of the camera.

The condenser has been enclosed in a glass box to minimize the effect of the wind on the falling aggregates. However, for the day analyzed in this work, the meteorological station placed next to the apparatus showed basically no wind that day (< 0.1 m/s).

Evaluation of the electric field inside the copper plate by means of an electric field mill

The magnitude of $\vec{E}_{\text{int}}$ can be derived from the direct measurement of the field outside the plates, $\vec{E}_{\text{ext}}(x)$, expressed as a function of the x coordinate (i.e., perpendicular to the plane). $|\vec{E}_{\text{ext}}|$ has been measured using an electric field mill Statometer II HAUG. The key point of the technique is that the external measurement of $|E_{\text{ext}}(x)|$ can be associated with the potential difference inside the capacitor (ΔV) by means of the analytical expression of Parker (*47*), where for a condenser of finite L and W, it reads as follows

$$|E_{\text{ext}}(x)| = \Delta V \cdot \frac{2\,L\,W(L^2 + W^2 + 8x^2)}{\pi\,(L^2 + 4x^2)\,(W^2 + 4x^2)\sqrt{L^2 + W^2 + 4x^2}} \quad (5)$$

Under the approximation of infinite parallel plate capacitor (i.e., $E_{\text{int}} \approx$ constant) the electric field inside the capacitor can be then evaluated as $E_{\text{int}} \approx \frac{\Delta V}{d}$, where $d = 1.8 \pm 0.3$ cm is the distance between the plates. The potential differences evaluated for the positive and the negative plates, respectively, are $\Delta V_+ = 10.6 \pm 2.2$ kV and $\Delta V_- = 7.8 \pm 1.7$ kV. The two values can be combined into a single weighted average $\Delta V = 8.9 \pm 1.3$ kV (see section S5). The best estimate for E_{int} using the propagation of uncertainties is $E_{\text{int}} = 495 \pm 73$ kV m^{-1}.

Determination of the electric field by means of the motion of a conductive sphere inside the copper plates

A direct measurement of $\vec{E}_{\text{int}}$ can be done by inverting the motion of a conductive sphere of mass m_s and radius R_s located inside the capacitor. We applied this methodology before and during the tephra fallout, recording the oscillatory motion of a conductive sphere of mass $m_s = 0.7$ g and radius $R_s = 0.5$ cm by means of a Phantom M110 HSC with framerate of 1500 fps (i.e., $\Delta t = 667$ μs). This methodology provides a completely independent estimation of the electric field in respect to measurement with the electric field mill. $\vec{E}_{\text{int}}$ initially induces a polarization on the surface of the sphere creating an asymmetry on the distribution of charges. This drives the initial movement of the sphere toward one of the two plates depending on the initial conditions of the problem. Regardless the initial induction, when the metal sphere touches the plate, it acquires a net charge Q_0 that can be expressed as a function of E_{int} by means of the image charge method

$$Q_0 = \frac{2}{3}\pi^3 \varepsilon_a R_s^2 E_{\text{int}} \quad (6)$$

where ε_a is the absolute electrical permittivity of air ($\varepsilon_a = \varepsilon_r \cdot \varepsilon_0 = 8.859 \cdot 10^{-12}$F m^{-1}). Equation 6 allows expressing the electric force on the sphere ($\vec{F}_e = E_{\text{int}}\hat{x}$) only as a function of the unknown electric field E_{int} (see section S6). Starting from the trajectories recorded using the HSC is thus possible to constrain E_{int} from inverting the equation of motion of the sphere as explained in section S6, where the full description of the procedure is reported. Two independent datasets have been recorded just before the eruption and during the tephra fallout, hereafter named, respectively, as dataset A and dataset B. Dataset A is made of an oscillatory motion made of 21 single trajectories. Dataset B is made of 50 single trajectories but characterized by a larger variability respect to dataset A. This is due to the more difficult conditions of the experiment during the ash fallout and some oscillations of the pendulum in the perpendicular plane of the camera at the moment of the video recording. The final evaluation of the electric fields is, respectively, $E_{\text{int\_A}} = 591 \pm 5$ kV m^{-1}for the dataset A and $E_{\text{int\_B}} = 630 \pm 21$ kV m^{-1} for dataset B.

Combination of independent measurements to provide the final estimation of the electric field inside the plates

In the previous sections, we discussed two independent techniques to estimate the electric field $\vec{E}_{\text{int}}$ inside the copper plates. The first methodology consists in a direct measurement of the electric field outside the capacitor by means of an electric field mill and the use of the analytical expression reported in (*47*) to quantify the potential difference inside the plates. Then, the electric field $\vec{E}_{\text{int}}$ is derived under the assumption that the system can be approximated as an infinite plate capacitor. This technique gives $E_{\text{int\_mill}} = 495 \pm 73$ kV m^{-1}.

The second methodology relies on the inversion of the equation of motion of a conductive sphere that follows an oscillatory motion due to the presence of the electric field inside the condenser. This technique has been applied to two different datasets (dataset A and dataset B) recorded using an HSC just before the volcanic eruption and during the tephra fallout. The electric field inside the copper plates evaluated with this technique is $E_{\text{int\_A}} = 591 \pm 5$ kV m^{-1} for dataset A and $E_{\text{int\_B}} = 630 \pm 21$ kV m^{-1} for dataset B.

Following Taylor (*48*), the three estimations can be combined in a weighted mean that takes into account the relative importance of each uncertainty. This gives a final value for the internal electric field $\overline{E}_{\text{int}} = 592 \pm 7$ kV m^{-1} (relative error ≈1%). An alternative and more precautionary approach considers the three independent estimations as totally equivalent and the global uncertainty as the lower and upper limits of the electric field spanned by the three measurements. This gives a final value of $\overline{E}_{\text{int}} = 572 \pm 113$ kV m^{-1} (relative error ≈ 20%) that will be used later on in the text.

Monte Carlo method for the determination of the electric charges on falling ash from HSC videos

The database collected 26 November 2019 is composed by $N_k = 47$ aggregates—44 were not broken by the electric field and 3 were broken. A Monte Carlo approach has been applied to the uncertainty propagation and the final evaluation of the net charge Q_p carried by single ash falling. In this methodology, the measured variables, such as the electric field ($\overline{E}_{\text{int}}$), the particle projected area (A_p), and particle velocity ($\vec{v}_p$), are expressed in terms of their statistical distributions (hereafter named as the parent distributions). Parent distributions for $\overline{E}_{\text{int}} = 572 \pm 113$ kV m^{-1} and $\vec{v}_A$ are Gaussian distributions with mean and SD assumed on the basis of the average and the SD calculated from field measurements or curve fitting. The parent distributions for A_A are well described in terms of a loglogistic distribution, derived by fitting the raw areas with the MATLAB built-in function histfit.

On the other hand, the aggregate bulk density (ρ_A), aggregate diameter (d_A), and aggregate mass (m_p) (hereafter named the dependent variables) are evaluated by randomly picking $N_{MC} = 20.000$ values from the parent distributions and solving for the following equations

$$\rho_A = \rho_f \cdot \left(1 + \frac{3}{4}\frac{C_D\, v_{Az}^2}{g\, d_A}\right) \quad (7)$$

$$d_A = \sqrt{\frac{4\, A_A}{\pi}} \quad (8)$$

$$m_A = \rho_A \frac{\pi}{6} d_A^3 \quad (9)$$

where C_D is the drag coefficient formula of Clift and Gauvin (*49*) and $\vec{v}_A = \vec{v}_{Ax} + \vec{v}_{Az}$. In this context, the $\hat{x}$ axis is parallel to the electric field, and the $\hat{z}$ axis is perpendicular to it (vertically oriented). The vertical velocity $\vec{v}_{Az}$ is measured in the portion of space above the copper plates, where the action of the electric field can be considered as negligible, and the aggregate is assumed to fall at its terminal velocity (i.e., $v_{Az} = v_t$). To do so, the FOV of the HSC is set to record both the copper plates and few centimeters of free space above them. Nevertheless, the measurements have confirmed that v_{Az} remains constant and equal to v_t also in the space within the HVCP. This proves that the electric field is well approximated by a vector oriented along the $\hat{x}$ axis. It is worth noticing that those aggregates that were broken by the electric field were all PC1 type aggregates. This is confirmed by the measurement of the aggregate density before the breaking and the images of their impact with the copper plates. For these aggregates, we assume that the aggregate density distribution before and after the breaking remains the same. This is a good approximation for PCs, for which the packing is assumed to be homogeneous and symmetrical in the volume (*49*). This assumption allows us to estimate the mass of the fragments.

For a given *i*th combination of the parameters ($i \in [1 \ldots N_{MC}]$), the charge Q_A is then found by inverting $N_Q = 2.000$ times the equation of motion along from the actual trajectory recorded with the HSC

$$m_p \frac{d\, v_{Ax}}{dt} = -\frac{1}{2}\rho_f C_D A_A v_{px}^2 + Q_A E_{int} \quad (10)$$

The N_Q values of Q_p are selected by picking random values from a uniform distribution that spans the interval $[-\sigma_{lim}, +\sigma_{lim}]$, where $\sigma_{lim} = 10^{-4}\mathrm{Cm}^{-2}$ (about three times the breakdown value for air at 1 atm). Equation 10 is solved using the MATLAB package ODE45, computing the initial conditions on both position and velocity from the recorder images. For a single combination of the Monte Carlo parameters ($i \in [1 \ldots N_{MC}]$), the best value for Q_A is found from the *j*th trajectory that minimizes the sum of distances between the *N* observed points (x_{Oi}, z_{Oi}) and the *N* computed ones (x_{Ci}, z_{Ci}).

The whole procedure is repeated N_{MC} times, and the final charge associated to the *k*th aggregate is described in terms of a statistical distribution, for which we use as descriptors the mode, the 5th and the 95th percentiles, respectively, for the most probable value of the charge and the uncertainty interval (90% confidence interval). In total, we performed $N_k \times N_{MC} \times N_Q \approx 2 \times 10^9$ inversions.

SUPPLEMENTARY MATERIALS

Supplementary material for this article is available at https://science.org/doi/10.1126/sciadv.abo7380

REFERENCES AND NOTES

1. S. F. Jenkins, T. M. Wilson, C. Magill, V. Miller, C. Stewart, R. Blong, W. Marzocchi, M. Boulton, C. Bonadonna, A. Costa, Volcanic ash fall hazard and risk, in *Global Volcanic Hazards and Risk*, S. C. Loughlin, S. Sparks, S. K. Brown, S. F. Jenkins, C. Vye-Brown, Eds. (Cambridge Univ. Press, 2015), pp. 173–222.
2. R. J. Brown, C. Bonadonna, A. J. Durant, A review of volcanic ash aggregation. *Phys. Chem. Earth* **45-46**, 65–78 (2012).
3. P. Lechner, A. Tupper, M. Guffanti, S. Loughlin, T. Casadevall, Volcanic ash and aviation: The challenges of real-time, global communication of a natural hazard, in *Observing the Volcano World: Volcano Crisis Communication*, C. J. Fearnley, D. K. Bird, K. Haynes, W. J. McGuire, G. Jolly, Eds. (Springer International Publishing, 2018), 51–64.
4. S. D. Egan, M. Stuefer, P. W. Webley, T. Lopez, C. F. Cahill, M. Hirtl, Modeling volcanic ash aggregation processes and related impacts on the April-May 2010 eruptions of Eyjafjallajökull volcano with WRF-Chem. *Nat. Hazards Earth Syst. Sci.* **20**, 2721–2737 (2020).
5. L. Mastin, M. Pavolonis, S. Engwell, R. Clarkson, C. Witham, G. Brock, I. Lisk, M. Guffanti, A. Tupper, D. Schneider, F. Beckett, T. Casadevall, G. Rennie, Progress in protecting air travel from volcanic ash clouds. *Bull. Volcanol.* **84**, 9 (2022).
6. R. Schumacher, H. U. Schmincke, Models for the origin of accretionary lapilli. *Bull. Volcanol.* **56**, 626–639 (1995).
7. M. R. James, J. S. Gilbert, S. J. Lane, Experimental investigation of volcanic particle aggregation in the absence of a liquid phase. *J. Geophys. Res. Solid Earth* **107**, 13 (2002).
8. M. R. James, S. J. Lane, J. S. Gilbert, Density, construction, and drag coefficient of electrostatic volcanic ash aggregates. *J. Geophys. Res. Solid Earth* **108**, 12 (2003).
9. C. Bonadonna, R. Genco, M. Gouhier, M. Pistolesi, R. Cioni, F. Alfano, A. Hoskuldsson, M. Ripepe, Tephra sedimentation during the 2010 Eyjafjallajökull eruption (Iceland) from deposit, radar, and satellite observations. *J. Geophys. Res. Solid Earth* **116**, B12202 (2011).
10. C. Cimarelli, M. A. Alatorre-Ibarguengoitia, U. Kueppers, B. Scheu, D. B. Dingwell, Experimental generation of volcanic lightning. *Geology* **42**, 79–82 (2014).
11. S. Alois, J. Merrison, J. J. Iversen, J. Sesterhenn, Contact electrification in aerosolized monodispersed silica microspheres quantified using laser based velocimetry. *J. Aerosol Sci.* **106**, 1–10 (2017).
12. S. Stern, C. Cimarelli, D. Gaudin, B. Scheu, D. B. Dingwell, Electrification of experimental volcanic jets with varying water content and temperature. *Geophys. Res. Lett.* **46**, 11136–11145 (2019).
13. J. Méndez Harper, L. Courtland, J. Dufek, J. McAdams, Microphysical effects of water content and temperature on the triboelectrification of volcanic ash on long time scales. *J. Geophys. Res. Atmos.* **125**, e2019JD031498 (2020).
14. S. Pollastri, E. Rossi, C. Bonadonna, J. P. Merrison, Modelling the effect of electrification on volcanic ash aggregation. *Front. Earth Sci.* **8**, 574106 (2021).
15. M. Z. U. Jacobson, *Fundamentals of Atmospheric Modeling* (Cambridge Univ. Press, 2005).
16. C. Cimarelli, M. A. Alatorre-Ibargüengoitia, K. Aizawa, A. Yokoo, A. Díaz-Marina, M. Iguchi, D. B. Dingwell, Multiparametric observation of volcanic lightning: Sakurajima Volcano, Japan. *Geophys. Res. Lett.* **43**, 4221–4228 (2016).
17. C. M. Smith, D. Gaudin, A. R. van Eaton, S. A. Behnke, S. Reader, R. J. Thomas, H. Edens, S. R. McNutt, C. Cimarelli, Impulsive volcanic plumes generate volcanic lightning and vent discharges: A statistical analysis of Sakurajima volcano in 2015. *Geophys. Res. Lett.* **48**, e2020GL092323 (2021).
18. M. S. Briggs, S. Lesage, C. Schultz, B. Mailyan, R. H. Holzworth, A terrestrial gamma-ray flash from the 2022 Hunga Tonga–Hunga Ha'apai volcanic eruption. *Geophys. Res. Lett.* **49**, e2022GL099660 (2022).
19. D. A. Yuen, M. A. Scruggs, F. J. Spera, Y. Zheng, H. Hu, S. R. McNutt, G. Thompson, K. Mandli, B. R. Keller, S. S. Wei, Z. Peng, Z. Zhou, F. Mulargia, Y. Tanioka, Under the surface: Pressure-induced planetary-scale waves, volcanic lightning, and gaseous clouds caused by the submarine eruption of Hunga Tonga-Hunga Ha'apai volcano. *Earthquake Res. Adv.* **2**, 100134 (2022).
20. T. A. Mather, R. G. Harrison, Electrification of volcanic plumes. *Surv. Geophys.* **27**, 387–432 (2006).
21. C. Cimarelli, K. Genareau, A review of volcanic electrification of the atmosphere and volcanic lightning. *J. Volcanol. Geotherm. Res.* **422**, 107449 (2022).
22. J. Méndez Harper, J. Dufek, The effects of dynamics on the triboelectrification of volcanic ash. *J. Geophys. Res. Atmos.* **121**, 8209–8228 (2016).
23. M. R. James, S. J. Lane, J. S. Gilbert, Volcanic plume electrification: Experimental investigation of a fracture-charging mechanism. *J. Geophys. Res. Solid Earth* **105**, 16641–16649 (2000).
24. J. Mason, The generation of electric charges and fields in thunderstorms. *Proc. Math. Phys. Eng. Sci.* **415**, 303–315 (1988).
25. T. W. Woods, K. Genareau, K. L. Wallace, Influence of grain size and shape on volcanic ash electrical conductivity. *J. Volcanol. Geotherm. Res.* **393**, 106788 (2020).
26. H. Hatakeyama, On the disturbance of the atmospheric electric field caused by the smoke-cloud of the volcano asama-yama. *Pap. Meteorol.Geophys.* **8**, 302–316 (1958).

27. J. S. Gilbert, S. J. Lane, R. S. J. Sparks, T. Koyaguchi, Charge measurements on particle fallout from a volcanic plume. *Nature* **349**, 598–600 (1991).
28. T. Miura, T. Koyaguchi, Y. Tanaka, Measurements of electric charge distribution in volcanic plumes at Sakurajima volcano Japan. *Bull. Volcanol.* **64**, 75–93 (2002).
29. A. Khayari, A. T. Perez, Charge acquired by a spherical ball bouncing on an electrode: Comparison between theory and experiment. *IEEE Trns. Dielectr. Electr. Insul.* **9**, 589–595 (2002).
30. O. V. Kim, P. F. Dunn, Real-time direct charge measurements of microdroplets and comparison with indirect methods. *Aerosol Sci. Tech.* **44**, 292–301 (2010).
31. A. M. Drews, C. A. Cartier, K. J. M. Bishop, Contact charge electrophoresis: Experiment and theory. *Langmuir* **31**, 3808–3814 (2015).
32. S. B. Mueller, U. Kueppers, J. Ametsbichler, C. Cimarelli, J. P. Merrison, M. Poret, F. B. Wadsworth, D. B. Dingwell, Stability of volcanic ash aggregates and break-up processes. *Sci. Rep.* **7**, 7440 (2017).
33. M. C. D. Vecino, E. Rossi, V. Freret-Lorgeril, A. Fries, P. Gabellini, J. Lemus, S. Pollastri, A. P. Poulidis, M. Iguchi, C. Bonadonna, Aerodynamic characteristics and genesis of aggregates at Sakurajima Volcano, Japan. *Sci. Rep.* **12**, 2044 (2022).
34. V. Lee, S. Waitukaitis, M. Miskin, H. M. Jaeger, Direct observation of particle interactions and clustering in charged granular streams. *Nat. Phys.* **11**, 733–737 (2015).
35. R. Beleca, M. Abbod, W. Balachandran, P. R. Miller, Investigation of electrostatic properties of pharmaceutical powders using phase doppler anemometry. *IEEE Trans. Ind. Appl.* **46**, 1181–1187 (2010).
36. G. Bagheri, E. Rossi, S. Biass, C. Bonadonna, Timing and nature of volcanic particle clusters based on field and numerical investigations. *J. Volcanol. Geotherm. Res.* **327**, 520–530 (2016).
37. P. Gabellini, E. Rossi, C. Bonadonna, M. Pistolesi, G. Bagheri, R. Cioni, Physical and aerodynamic characterization of particle clusters at Sakurajima volcano (Japan). *Front. Earth Sci.* **8**, 575874 (2020).
38. D. J. Lacks, A. Levandovsky, Effect of particle size distribution on the polarity of triboelectric charging in granular insulator systems. *J. Electrostat.* **65**, 107–112 (2007).
39. M. A. Bilici, J. R. Toth III, R. M. Sankaran, D. J. Lacks, Particle size effects in particle-particle triboelectric charging studied with an integrated fluidized bed and electrostatic separator system. *Rev. Sci. Instrum.* **85**, 103903 (2014).
40. S. Alois, J. Merrison, J. J. Iversen, J. Sesterhenn, Quantifying the contact electrification of aerosolized insulating particles. *Powder Technol.* **332**, 106–113 (2018).
41. J. Méndez Harper, C. Cimarelli, V. Cigala, U. Kueppers, J. Dufek, Charge injection into the atmosphere by explosive volcanic eruptions through triboelectrification and fragmentation charging. *Earth Planet. Sci. Lett.* **574**, 117162 (2021).
42. E. Bichoutskaia, A. L. Boatwright, A. Khachatourian, A. J. Stace, Electrostatic analysis of the interactions between charged particles of dielectric materials. *J. Chem. Phys.* **133**, 024105 (2010).
43. J. Méndez Harper, C. Helling, J. Dufek, Triboelectrification of KCl and ZnS particles in approximated exoplanet environments. *Astrophys. J.* **867**, 123 (2018).
44. S. J. Lane, J. S. Gilbert, M. Hilton, The aerodynamic behaviour of volcanic aggregates. *Bull. Volcanol.* **55**, 481–488 (1993).
45. E. Rossi, C. Bonadonna, SCARLET-1.0: SpheriCal approximation for viRtuaL aggrEgaTes. *Development* **14**, 4379–4400 (2021).
46. A. Várai, M. Vincze, J. Lichtenberger, M. Jànosi, Search for possible relationship between volcanic ash particles and thunderstorm lightning activity. *J. Phys. Conf. Ser.* **333**, 012016 (2011).
47. G. W. Parker, Electric field outside a parallel plate capacitor. *Am. J. Phys.* **70**, 502–507 (2002).
48. J. Taylor, *Introduction to Error Analysis, the Study of Uncertainties in Physical Measurements* (University Science Books, ed. 2, 1997).
49. R. Clift, W. H. Gauvin, Motion of entrained particles in gas streams. *Can. J. Chem. Eng.* **49**, 439–448 (1971).

Acknowledgments: We would like to thank the entire group that participated in the field campaign: V. Freret-Lorgeril, C. Diaz Vecino, J. Lemus, A. Fries, P. Gabellini, A. Poulidis, and M. Iguchi. A special and grateful mention goes to A. Fries and P. Gabellini for the help provided in the field on 26 November 2019 during the tephra fallout analyzed in this work. In addition, we thank G. Bagheri for constructive discussion. **Funding:** This work was supported by the Swiss National Science Foundation (grant number 200021_156255); field work of S.P. was funded by the Friedlander Foundation. **Author contributions:** Conceptualization: S.P. and E.R. Methodology: E.R. and S.P. Investigation: S.P. and E.R. Visualization: E.R., S.P., and C.B. Supervision: C.B. Writing—original draft: E.R. and S.P. Writing—review and editing: E.R., C.B., and SP. **Competing interests:** The authors declare that they have no competing interests. **Data and materials availability:** All data needed to evaluate the conclusions in the paper are present in the paper and/or the Supplementary Materials. The raw MATLAB database is available at the Zenodo repository: https://doi.org/10.5281/zenodo.7068143

Submitted 24 February 2022
Accepted 30 September 2022
Published 18 November 2022
10.1126/sciadv.abo7380